

# Spin and orbital excitations in undoped infinite layers: a comparison between superconducting PrNiO<sub>2</sub> and insulating CaCuO<sub>2</sub>

F. Rosa,<sup>1,\*</sup> H. Sahib,<sup>2,†</sup> G. Merzoni,<sup>1,3</sup> L. Martinelli,<sup>1,‡</sup> R. Arpaia,<sup>4,5</sup> N.B. Brookes,<sup>6</sup>  
D. Di Castro,<sup>7,8</sup> M. Zinouyeva,<sup>1</sup> M. Salluzzo,<sup>9</sup> D. Preziosi,<sup>2</sup> and G. Ghiringhelli<sup>1,10,§</sup>

<sup>1</sup>*Dipartimento di Fisica, Politecnico di Milano, piazza Leonardo da Vinci 32, I-20133 Milano, Italy*

<sup>2</sup>*Université de Strasbourg, CNRS, IPCMS UMR 7504, F-67034 Strasbourg, France*

<sup>3</sup>*European XFEL, Holzkoppel 4, Schenefeld, D-22869, Germany*

<sup>4</sup>*Department of Molecular Sciences and Nanosystems,  
Ca' Foscari University of Venice, I-30172 Venice, Italy*

<sup>5</sup>*Quantum Device Physics Laboratory, Department of Microtechnology and Nanoscience,  
Chalmers University of Technology, SE-41296 Göteborg, Sweden*

<sup>6</sup>*ESRF, The European Synchrotron, 71 Avenue des Martyrs, CS 40220, F-38043 Grenoble, France*

<sup>7</sup>*Dipartimento di Ingegneria Civile e Ingegneria Informatica,*

*Università di Roma Tor Vergata, Via del Politecnico 1, I-00133 Roma, Italy*

<sup>8</sup>*CNR-SPIN, Università di Roma Tor Vergata, Via del Politecnico 1, I-00133 Roma, Italy*

<sup>9</sup>*CNR-SPIN, Complesso Monte Sant'Angelo-Via Cinthia, I-80126 Napoli, Italy*

<sup>10</sup>*CNR-SPIN, Dipartimento di Fisica, Politecnico di Milano, I-20133 Milano, Italy*

(Dated: November 10, 2025)

Infinite-layer nickelates are among the most promising cuprate-akin superconductors, although relevant differences from copper oxides have been reported. Here, we present momentum- and polarization-resolved RIXS measurements on chemically undoped, superconducting PrNiO<sub>2</sub>, and compare its magnetic and orbital excitations with those of the reference infinite layer cuprate CaCuO<sub>2</sub>. In PrNiO<sub>2</sub>, the in-plane magnetic exchange integrals are smaller than in CaCuO<sub>2</sub>, whereas the out-of-plane values are similar, indicating that both materials support a three-dimensional antiferromagnetic order. Orbital excitations, associated to the transitions within *3d* states of the metal, are well reproduced within a single-ion model and display similar characteristics, except for the Ni-*d<sub>xy</sub>* peak which, besides lying at significantly lower energy, shows an opposite dispersion to that of Cu-*d<sub>xy</sub>*. This is interpreted as a consequence of orbital superexchange coupling between nearest neighbor sites, which drives the orbiton propagation. Our observations demonstrate that infinite-layer cuprates and nickelates share most of the spin and orbital properties, despite their markedly different charge-transfer energy  $\Delta$ .

DOI: 10.15151/ESRF-ES-1430231833

## I. INTRODUCTION

The quest for high- $T_c$  superconductivity has brought to the attention of the condensed matter community the wide family of strongly correlated materials [1–3]. Infinite-layer (IL) nickelates recently gained strong interest [4–11] thanks to their apparent analogies with cuprates, including a square lattice-based structure dominated by superexchange antiferromagnetic interaction [12, 13] and the emergence of superconductivity upon hole doping. So far, the latter has been observed only in thin films [14–18] which makes it difficult to assess the magnetic structure of the IL nickelate system, as no direct correspondence with the bulk can be established. The bulk is mostly characterized by the absence of long-range order and the presence of a spin-glass behavior [13, 19, 20]. Conversely, evidence of spin-spin correlations was reported from extensive Resonant Inelastic X-ray Scattering (RIXS) [12, 21], as well as, X-ray Magnetic Circular Dichroism (XMCD) [22] experiments in superconducting and non superconducting thin films.

On the other hand, the analogies between cuprates and IL nickelates [6, 23] are not yet sufficient to prove the existence of a single underlying mechanism for unconventional superconductivity [7, 24, 25], but rather urge further investigation. At the root of the observed affinities is the common  $3d^9$  electronic configuration of Cu<sup>2+</sup> and Ni<sup>1+</sup> ions occupying the corners of a planar spin 1/2 square lattice, with oxygen ligands along the edges. However, when referring to the Zaanen-Sawatzky-Allen scheme [26], cuprates are classified as Charge-Transfer (CT) insulators and IL nickelates as Mott-Hubbard insulators, because the ligand-to-metal charge-transfer energy  $\Delta$  is smaller/larger than

\* francesco.rosa@polimi.it

† Present address: Department of Physics, College of Science, University of Halabja, Halabja, Iraq

‡ Present address: Physik-Institut, Universität Zürich, Winterthurerstrasse 190, CH-8057 Zürich, Switzerland

§ giacomo.ghiringhelli@polimi.it

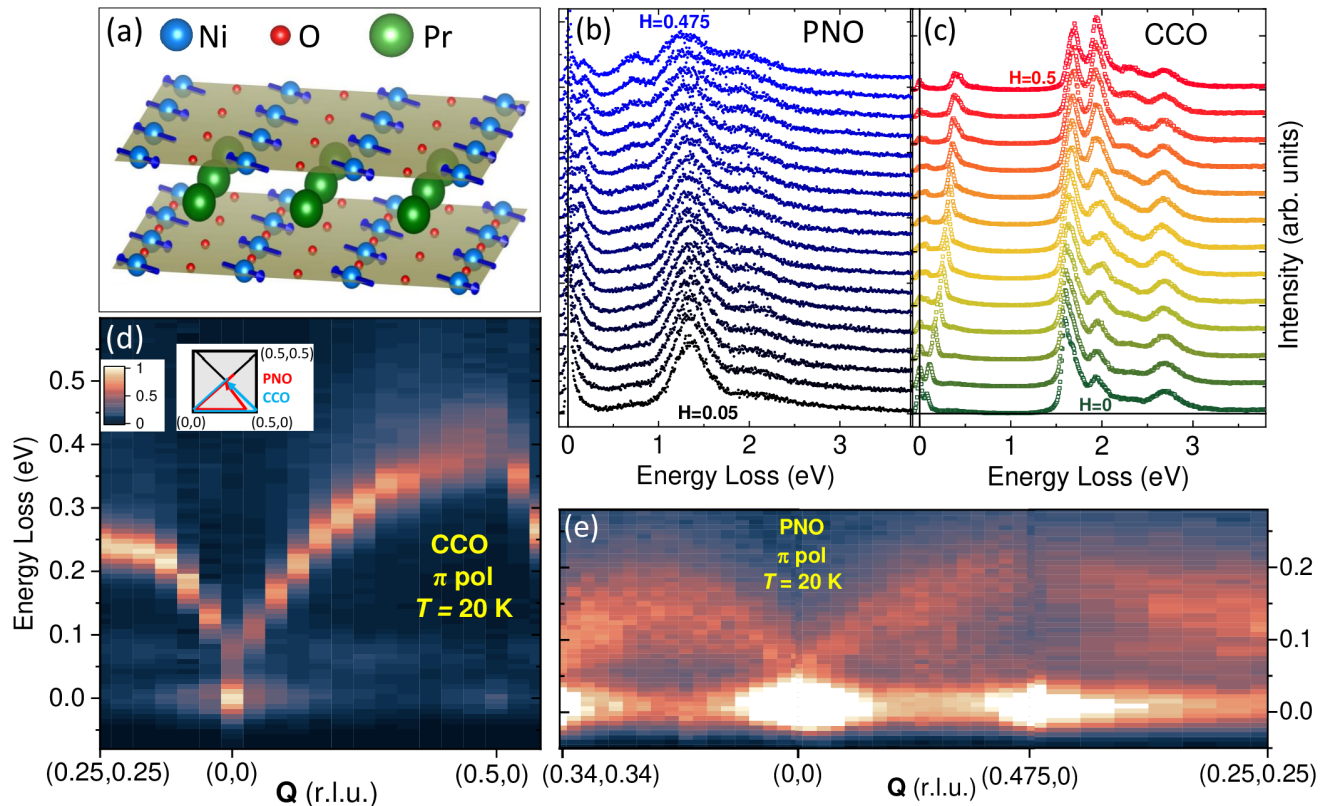


FIG. 1. **Comparison of RIXS spectra on PNO and CCO.** (a) Infinite-layer structure (ochre planes) of PNO, showing the local tetragonal coordination of the nickel atoms to the surrounding oxygens; CCO has the same structure, with Ni and Pr replaced by Cu and Ca respectively; the dark blue arrows on metal sites depict antiferromagnetic spin order. (b-c) RIXS spectra stacks for PNO and CCO respectively, along the  $[H, 0]$  cut of the Brillouin zone. (d-e) Momentum-dependent RIXS maps of CCO (d) and PNO (e) along the triple paths of the Brillouin zone shown in the (d) inset for the two samples. All (d-e) spectra have been normalized to the  $dd$  energy integral along the interval (1; 3.5) eV.

the Coulomb repulsion  $U$  respectively [4, 8, 11, 21, 27]. Consequently, in IL nickelates the oxygen  $2p$  band lies far below the Fermi level and the doping holes are mostly residing on the metal sites, at variance with other nickel oxides, where  $\Delta$  is small or even negative [28]. Whereas oxygen states contribute minimally to the DOS close to the Fermi level, according to the theory the rare-earth  $5d$  states in IL nickelates provide pockets across  $E_F$  [11, 17, 24, 29] which can inject extra holes even in nominally undoped compounds, a phenomenon known as self-doping [8, 30–32]. In fact, the degree of rare-earth hybridization with the Ni  $3d$  bands is still controversial [8, 33], and recent angle-resolved photoemission measurements did not provide evidence of electron pockets at the  $\Gamma$  point [34, 35].

As for magnetic properties, spin fluctuations are considered to play a major role in the formation of Cooper pairs in cuprates [36, 37], and a coexistence of magnetism and superconductivity has been suggested by XMCD [22], as well as muon spin rotation/relaxation in cuprates and IL nickelates [38, 39]: therefore, a comparative investigation by other methods is timely.

Here, we used RIXS to investigate the dynamical spin response of the nominally undoped though superconducting IL nickelate  $\text{PrNiO}_2$  (PNO) [40] and compare it to that of  $\text{CaCuO}_2$  (CCO) [41, 42], which has similar crystalline structure but fully insulating properties. In spite of self-doping and superconductivity, in PNO the spin excitation peak is sharp and disperses similarly to CCO. We find that the in-plane exchange integrals are smaller in PNO than in CCO, consistently with previous reports [12], while the out-of-plane values are comparable. Polarization-resolved RIXS reveals a better agreement of the PNO orbital excitations ( $dds$ ) with single-ion cross-section calculations, while in CCO a fourth peak occurs, whose origin remains unclear. Interestingly, the  $d_{xy}$  peak displays an opposite dispersion in the two materials, which we interpret as a consequence of distinct orbital superexchange couplings driving the orbital propagation in the two materials: nearest neighbor for the nickelate, next-nearest neighbor for the cuprate [43].

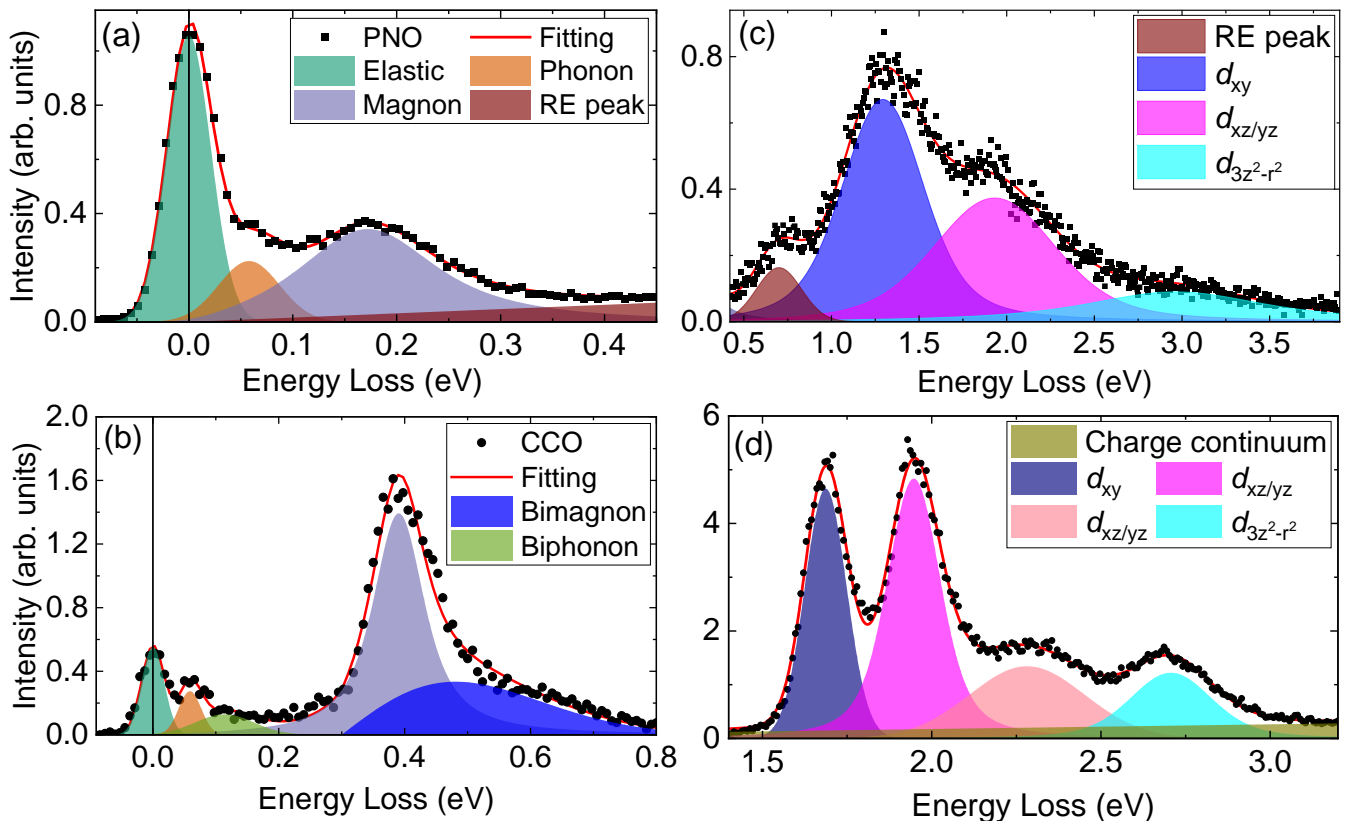


FIG. 2. **Analysis of RIXS spectra.** (a) Fitting of PNO spectrum with  $\pi$  incident polarization, as described in the main text. Data points were obtained as the sum of different spectra along  $[H, 0]$  with  $H$  between 0.4 and 0.475 r.l.u. at incident energy 852.48 eV. (b) Same fit for CCO, with  $H = 0.465$  r.l.u.; a second Gaussian is added here (light green) representing the phonon overtone, while the rare-earth peak tail has been replaced by the bimagnon continuum (dark blue). Elastic, phonon and magnon colors are the same as in (a). (c-d) Same fittings as (a-b) respectively, but focusing on the orbital excitations area.

## II. RESULTS AND DISCUSSION

Figure 1 displays an overview of RIXS spectra for both samples, showcasing orbital and spin excitations. The common IL structure is depicted in panel (a) together with the antiferromagnetic spin lattice. Panels (b-c) report spectra taken at different transferred momenta along the  $[H, 0]$  cut of the 2D reciprocal space. The orbital ( $dd$ ) excitations at high energy range (1-3 eV) show a small but significant dispersion as a function of the in-plane momentum, as discussed below [43, 44]. The sharp feature dispersing up to  $\sim 200$  meV in PNO and  $\sim 400$  meV in CCO is assigned to  $\Delta S = 1$  spin excitations, in agreement with previous RIXS results [12, 45–50]. These spin excitations follow a single-magnon dispersion across most of the reciprocal space along the M- $\Gamma$ -X path (panels d-e). Whereas the sharpness of the magnetic peak in CCO is a direct consequence of the long-range antiferromagnetic (AFM) order of the undoped compound [50, 51], the coexistence of superconductivity and sharp spin excitations in IL nickelates demonstrates the mild effect of self-doping on magnetism. This constitutes an important difference with respect to cuprates, where the chemical hole doping, required for superconductivity, quickly disrupts spin order and progressively smears the magnon excitation peak [49] across the superconducting dome (see below for a more quantitative comparison). Our observations are consistent with the muon spin rotation measurements in superconducting IL nickelates by Fowlie et al. [39], which hint at a similar coexistence. A recent debate was sparked by the observation of an elastic intensity increase around the quasi-commensurate wavevector  $Q \sim (0.33, 0)$ . This was first interpreted as an evidence of charge order analogous to the Charge Density Waves observed in cuprates [45, 52, 53], but later dismissed as resulting from periodic arrangement of residual apical oxygens from incomplete topotactic reduction [54]. Our integrals of the spectral weight in the quasielastic region, displayed in Figure S6 of the Supplementary Material, show no evidence of such an increase, confirming the absence of charge order in our samples and the fully occurred topotactic reaction.

In order to determine the energy of the magnetic excitations, we fitted the elastic and phonon peaks with resolution-limited Gaussian functions, and the magnetic peak with the damped harmonic oscillator spectral shape, convolved

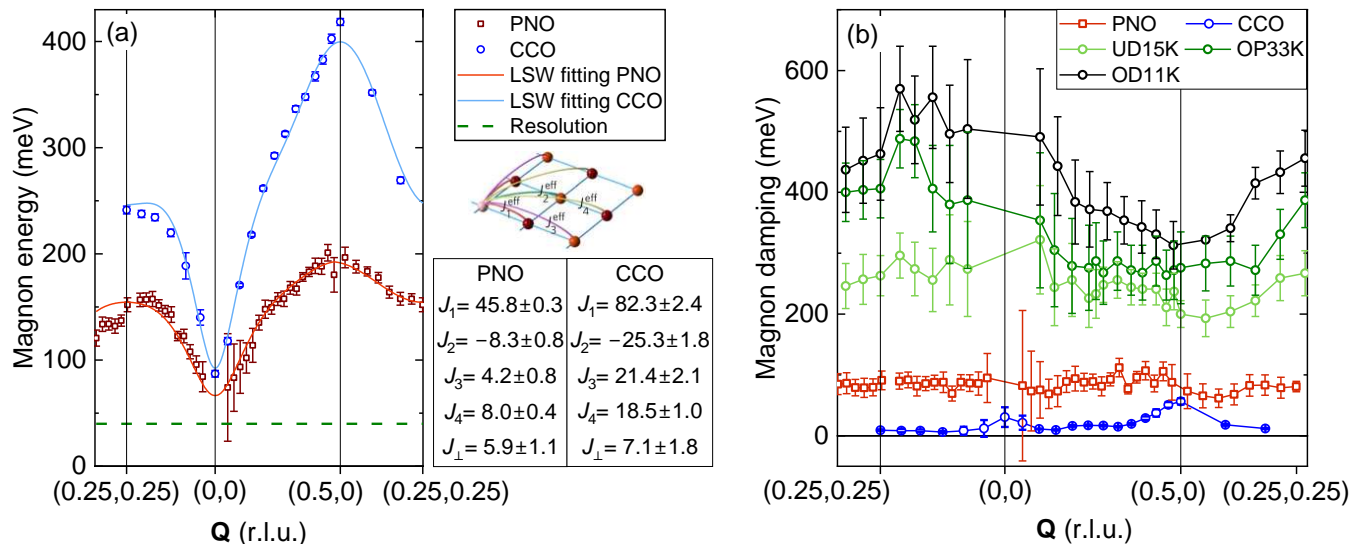


FIG. 3. **Comparison of magnon energy and damping.** (a) Fitting of dispersions of PNO and CCO with the Linear Spin Wave model fit. The definitions and values (in meV) of the four in-plane exchange coupling constants are displayed on the right [48]. (b) Comparison of the damping coefficients of PNO and CCO with those extracted from analogous fittings on Bi2201 cuprate at different doping levels in Ref. 49 (UD = underdoped, OP=optimally doped, OD=overdoped). Error bars in both panels represent 95% confidence intervals from the fittings.

with a Gaussian accounting for the experimental resolution [49] (see Figure 2(a-b)). A phonon peak at  $\sim 80$  meV must be considered in the fitting of the spectra; phonon and magnon overtones are only included in the cuprate fit, because in the nickelate these features are too close in energy and too broad. A similar fit was performed on the high-energy peaks related to the orbital transitions between  $3d$  levels (Panels (c-d), to be discussed in the following). More details about the fittings are available in the Supplementary Information IV. The momentum-energy dispersions for PNO and CCO are reported in Figure 3(a), while 3(b) shows a comparison between the extracted damping coefficients, related to the spectral broadening of the magnon, and the corresponding values for superconducting  $(\text{Bi,Pb})_2(\text{Sr,L a})_2\text{CuO}_{6+\delta}$  (Bi2201) samples at different doping levels, taken from Ref. 49. The peak broadening for the nickelate is found to be nearly constant ( $\sim 100$  meV) over the explored momentum range: such value is obviously larger than for CCO, where long-range AFM order provides almost undamped spin wave propagation. At the same time, it is less than half the corresponding value for the lowest doping level of superconducting Bi2201 ( $\gtrsim 200$  meV, within the confidence intervals). This demonstrates that self-doping has a much milder impact on spin order than chemical doping, endowing IL nickelates with a non-disruptive way to achieve superconductivity which is totally absent in copper oxides.

We notice also an increase of the elastic intensity around the X point, a result previously reported, but not discussed, for PNO and  $\text{NdNiO}_2$  [12, 47]. Upon approaching the X point in (0.5,0), the spin excitation becomes less intense and its shape is not an individual peak directly identified with a single magnon, as a consequence of fractionalization phenomena, related to the square lattice and independent of the material [55], and of multi-magnon excitations [56]. At the same time a continuum, possibly due to spinon pairs, appears and becomes increasingly intense towards the X point: for CCO these effects are very evident and were previously discussed by Martinelli et al. [50]. For PNO and other IL nickelates the broadening is harder to determine but the loss of intensity was previously observed [47]. We consider that here a single-peak fit is accurate enough for our purpose, although for CCO it results in an overestimation of the single-magnon damping energy close to (0.5,0) as shown in Figure 3(a).

To analyze the differences between the two samples, we fitted the extracted dispersion curves with those predicted by Linear Spin Wave theory (LSW) [57], computed using the SpinW library in Matlab [58]. We considered four in-plane exchange couplings  $J_{1-4}$  and one out-of-plane coupling  $J_\perp$ , similarly to what was done for CCO in Ref. 48. This is a novelty for IL nickelates, whose magnon dispersion was fitted with purely bidimensional LSW models so far [12, 47, 59, 60] or, at most, with an out-of-plane magnetic anisotropy [61] that, however, is hard to determine from RIXS spectra. We decided to add  $J_\perp$  because, when approaching the  $\Gamma$  point at non-integer  $L$  values, the single-magnon energy remains large, in strong analogy to the CCO case. The values of the extracted exchange  $J_s$  (in meV) are reported in Figure 3(a). The nearest-neighbor exchange  $J_1$  is about twice as large in CCO (82 meV) than in PNO (46 meV), in agreement with the literature [12, 24, 46]. On contrast,  $J_\perp$  is comparable in the two compounds (7 meV for CCO and 6 meV for PNO), leading to out-to-in-plane exchange ratio  $J_\perp/J_1$  of 8.5% for CCO

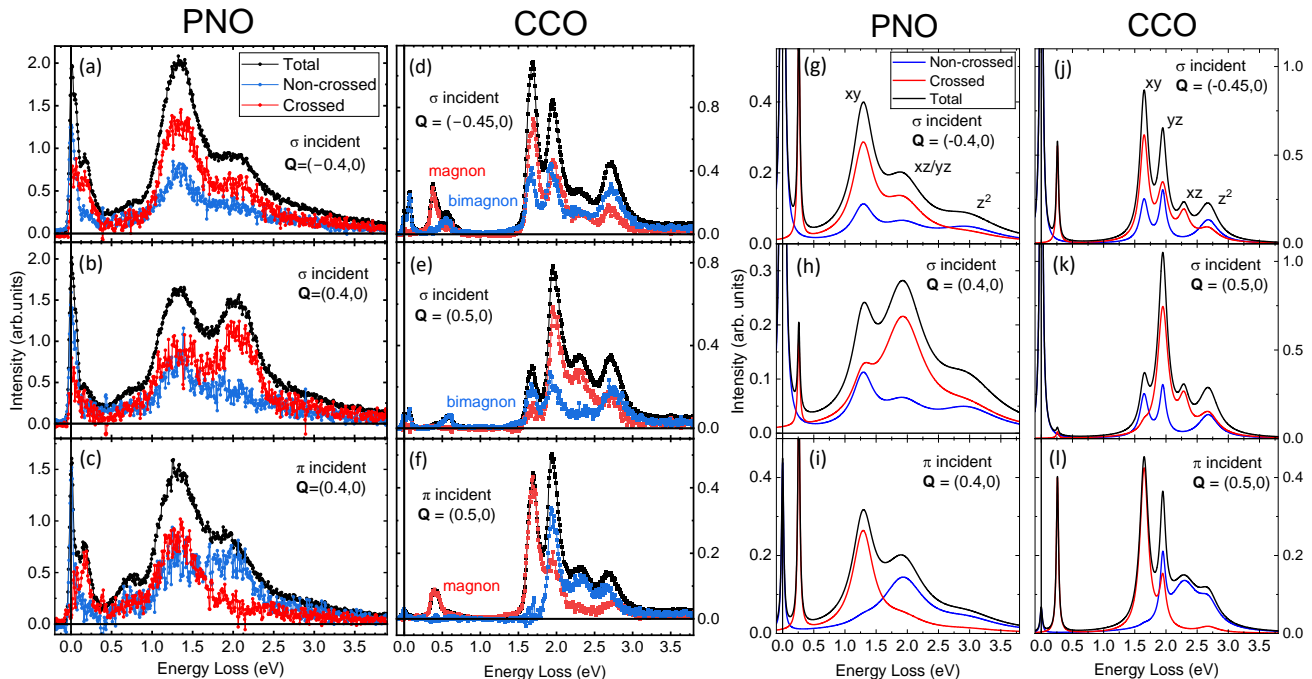


FIG. 4. **Comparison between polarimetric RIXS data and theory.** (a-f) Polarization-resolved RIXS spectra for PNO (a-c) and CCO (d-f), measured under the geometry and polarization conditions specified into each panel. (g-l) Corresponding single-ion RIXS cross-section calculations for the same polarization and geometry conditions as in (a-f), respectively.

and 13% for PNO. We notice that these values of  $J_{\perp}$  are close to the intra-unit-cell coupling of bi-layer cuprates like YBCO [48]. The absence of apical oxygens in IL nickelates leads to long-range, in-plane hopping similar to cuprates', despite the larger  $\Delta$  and the Mott-Hubbard character of the correlation gap. We observe that the 3D character of the spin-spin correlation is also similar in the IL nickelates and in the CCO, as testified by the comparable value of the spin excitation energy at in plane-zone center and non-integer  $L$  (60-80 meV respectively). Those analogies coexist with a markedly different degree of out-of-plane hybridization, introduced by the rare-earth ions separating the  $\text{NiO}_2$  planes in infinite-layer nickelates, in contrast to the negligible effect of Ca or Ba ions in cuprates. Also, they give a proof of the fully occurred topotactic reduction of the PNO samples and the absence of interstitial oxygen atoms.

Along the  $[H, H]$  direction we notice that the maximum of the dispersion in PNO is not at the BZ boundary  $(0.25, 0.25)$  r.l.u., but rather at  $(0.2, 0.2)$  r.l.u., and that the elastic peak intensity increases very much beyond the BZ boundary in  $(0.25, 0.25)$  r.l.u. (see Figure 1(e)). These facts might suggest the presence of an incommensurate resonant diffraction reflection distinct from the AFM  $(0.5, 0.5)$  point, which cannot be reached in RIXS due to kinematic limitations. Those peculiarities had already been observed but not discussed in Ref. 47 for PNO and  $\text{LaNiO}_2$ . Together with the elastic peak at  $(0.5, 0)$ , the anomalies observed along the  $[H, H]$  direction might indicate the presence of a 2D symmetry-breaking mechanism, such as stripe order, with complex phenomenology due to the interplay with the 3D magnetic structure. An investigation of this hypothesis falls beyond the scope of the present article.

To gain further insights, we measured RIXS spectra with analysis of the linear polarization of the scattered photons. We chose large momenta in the  $[H, 0]$  direction, with both positive and negative values of  $H = \pm 0.4$  r.l.u. for PNO and  $H = \pm 0.5$  r.l.u. for CCO. For positive  $H$  values we took both  $\sigma$  and  $\pi$  incident polarization, for negative  $H$  only the  $\sigma$  polarization was used because cross-sections for  $\pi$  incidence are much smaller [44]. The results are shown in Figure 4, where the spectral components with scattered polarization orthogonal to the incident one ( $\sigma\pi'$  and  $\pi\sigma'$ , i.e., crossed polarization) are given in red and those with parallel polarization ( $\sigma\sigma'$  and  $\pi\pi'$ ) are in blue. In Figure 4(c)-(f), we see that the single magnon peak at positive  $H$  has crossed character for both samples, in agreement with literature on cuprates [50, 62] and with theory [44, 63]. With  $\sigma$ -polarized incident light and positive  $H$ , the magnetic peak in CCO is purely parallel, consistently with the transfer of an even number of angular-momentum units (bimagnon). In contrast, in the nickelate this feature — if present — is too weak and broad to be clearly distinguished (Panels (e) and (b), respectively). In all PNO spectra we see that an unpolarized continuum is present, likely resulting from self-doping, which leads to a not purely crossed polarization character of the magnon in panel (c) and of the phonon peak in all spectra.

Orbital peak (eV)	PNO	CCO
$d_{xy}$	$1.29 \pm 0.02$	$1.65 \pm 0.02$
$d_{xz/yz}$	$1.93 \pm 0.06$	$1.95 \pm 0.01$
		$2.29 \pm 0.06$
$d_{z^2}$	$2.96 \pm 0.58$	$2.68 \pm 0.04$

TABLE I. **Orbital peaks energies (in eV) for PNO and CCO.** Energy losses of the  $dd$  peaks at BZ edge as extracted from the fittings in Figure 2(c-d).

The differences between the two samples are more evident in the  $dds$  spectral region (1-3 eV). Here the peaks have been fitted as already shown in Figure 2(c-d), and assigned according to the known crystal field splitting of  $3d$  orbitals in a square tetragonal environment [44]. Disregarding the peak at 0.7 eV in PNO, the lowest energy feature can be assigned to the  $d_{xy}$  orbital excitation in both samples. The energy position obtained by a multi-peak fitting is 1.29 eV and 1.65 eV for PNO and CCO respectively, with the difference likely being due to the different hopping parameters and in-plane lattice constants of the two materials, which are also grown on different substrates. The  $d_{xz/yz}$  excitation in the cuprate appears split into two components; again this phenomenon has been already observed [43] but not explained in CCO, although it might not be due to simple splitting between the single  $d_{xz}$  and  $d_{yz}$  features (see also the comparison with cross-sections explained below). Nevertheless, the  $d_{xz/yz}$  energy position is quite similar between the two systems (1.93 eV for PNO, 2.05 eV for the center of mass of the two features of CCO). The  $d_{z^2}$  feature, though less defined, has a possibly larger energy in the nickelate than in the cuprate. Polarization analysis shows that the  $d_{xz/yz}$  features have similar character for PNO and CCO in all three geometries, while the  $d_{xy}$  peak is similar at negative  $H$  but is very different at positive  $H$ . In fact, for  $H > 0$  it has almost pure crossed character for  $\pi$  and parallel character for  $\sigma$  for CCO but it is of mixed polarization character for PNO. A possible intuitive explanation is the proximity of the 0.7 eV peak, which is fully unpolarized in all cases. Such peak has been theoretically assigned to Ni  $3d$ -rare earth  $5d$  hybridized states [12], thus the mixed polarization character of the 1.29 eV peak might be a hint of stronger hybridization of Pr  $5d$  with Ni  $3d_{xy}$  states than with the  $3d_{xz/yz}$  ones. However, recent photoemission measurements [35] have shown no evidence of rare-earth states close to the Fermi level, highlighting instead a predominating role of electrone-like interstitial  $s$  states, where electrons are delocalized over several voids and coexist with the Ni  $3d_{x^2-y^2}$  electrons. It is not excluded that such  $s$  states can also interact with the  $3d_{xy}$  states, which are oriented in the same plane as the  $3d_{x^2-y^2}$ : further investigation is required to verify this hypothesis.

By comparing polarimetric RIXS data with single-ion cross-sections calculations shown in panels (g-l), and based on the energies listed in Table I, almost all of the CCO spectra can be quite well reproduced. We added here a splitting of the  $d_{xz/yz}$  peak into the two separate  $d_{xz}$  and  $d_{yz}$  features, giving good agreement except for the grazing incidence case. On the other hand, for the PNO spectra the measured  $d_{xy}$  peak at  $H = 0.4$  for  $\sigma$ -polarized incident light appears significantly stronger than predicted by the calculations, which may indicate contributions from Pr  $5d$  and/or interstitial  $s$  states.

We conclude the comparison between the orbital excitations by examining their dispersion. If they have a perfectly local nature they should show no momentum dependence, and in most layered cuprates, this is indeed what has been observed [44, 62, 64]. For 1D cuprates it was theoretically proposed and experimentally observed [65, 66] that some dispersion can be attributed to an effective orbital exchange interaction ultimately ascribed to the Cu-O hopping and to 1D fractionalization, which allows orbitons to propagate independently from magnetic excitations (Kugel-Khomskii orbiton model) [67]. In 2D cuprates it has been shown theoretically that the mechanism is strongly frustrated by the antiferromagnetic spin order that would immediately dress the propagating orbital excitation with a trail of spin excitations. Such coupling between the magnetic and orbital degrees of freedom, which strongly hinders orbiton propagation by nearest neighbor (NN) orbital superexchange, is known as magnetic string effect [68, 69]. However, in CCO the dispersion of the  $d_{xy}$  state was recently observed: it is attributed to the large next-nearest neighbor (NNN) orbital superexchange, which allows the orbiton to propagate along the diagonal avoiding coupling to magnons [43]. In Figure 5(a-b) we show that in PNO the  $d_{xy}$  peak disperses as a function of momentum. In comparison to the CCO case (c-d), the dispersion has opposite sign but similar bandwidth: the energy is maximum (minimum) at  $\Gamma$  and decreases (increases) with momentum in both  $[H, 0]$  and  $[H, H]$  directions for PNO (CCO). By fitting the  $d_{xy}$  dispersion with a simple orbital superexchange dispersion relation (continuous lines in Figure 5(a)-(c)) [43]:

$$\epsilon_{\mathbf{k}} = 2J^{orb} \cos(k_x) \cos(k_y) \quad (1)$$

we retrieve a value of  $J^{orb} = -11 \pm 2$  meV for CCO and  $J^{orb} = 14 \pm 4$  meV for PNO. As already mentioned, the negative sign of the former has been interpreted in Ref. 43 as a NNN orbital superexchange process, directly

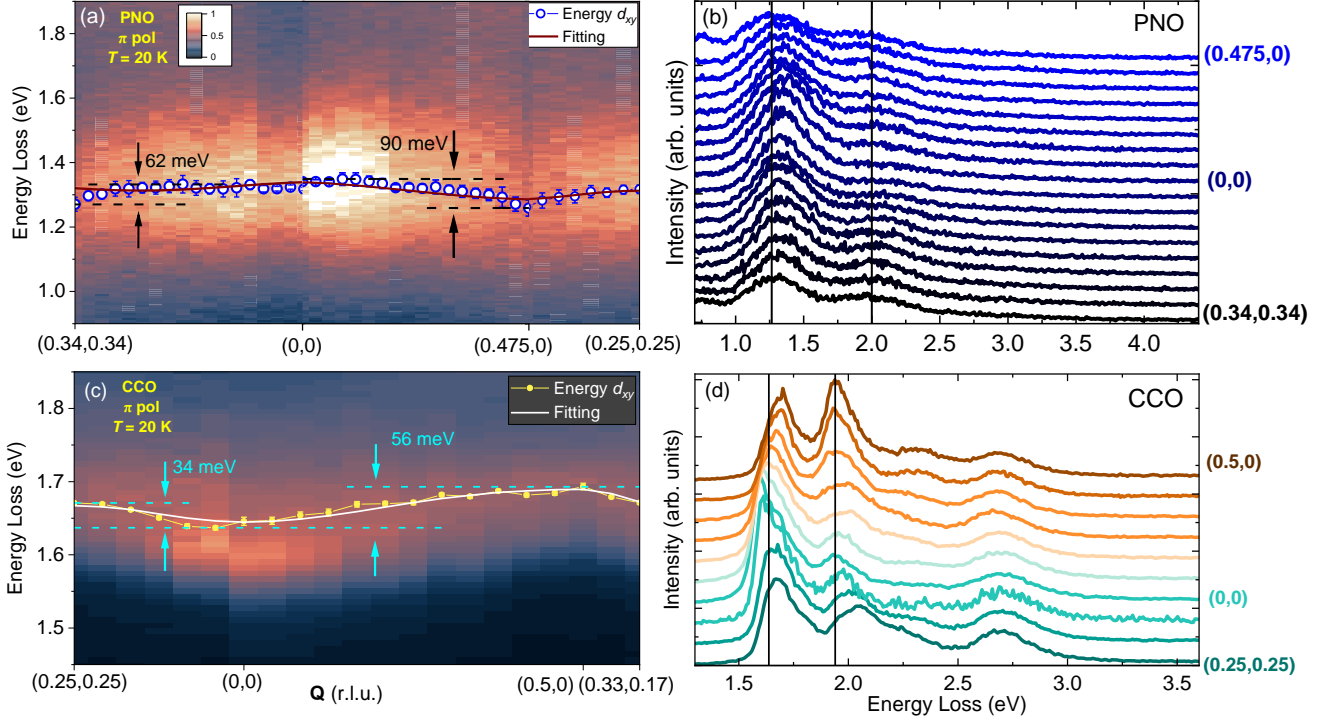


FIG. 5. **Orbital excitation dispersion.** (a) Momentum-resolved map in the  $d_{xy}$  energy range of PNO; dots highlight the dispersion of the peak, while the continuous line represents the charge transfer model fitting (see text). Horizontal dashed lines quote the maximum and minimum energies of each branch, with their distance being reported. The followed BZ cuts are the same shown in the inset of Figure 1(d). (b) Stack of spectra of PNO in the whole  $dd$  range, with vertical lines fixed at the minimum of the dispersion of the  $d_{xy}$  and  $d_{xz/yz}$  peak. (c-d) Same as (a-b), for CCO. Error bars in (a)-(c) represent 95% confidence intervals from the fittings.

connecting two metal sites on the opposite corners of a square. This is the dominating propagation path for collective orbital excitations in CCO, due to the strong hampering of NN superexchange by the orbital coupling to magnons. However, for PNO the positive sign of  $J^{orb}$  reveals a distinct behavior: since the nickelate, unlike the cuprate, does not present evidence of long-range AFM order, the magnetic string effect is expected to be absent or much weaker, and easily compensated by quantum fluctuations [68, 69]. The orbital NN superexchange, whose  $J^{orb}$  has an opposite sign to the NNN case, appears here as the dominating mechanism driving the orbital propagation.

To validate this hypothesis, we performed an estimation of NN and NNN couplings  $J^{orb}$  for the two materials according to a simple Hubbard-based charge transfer model. Details of the model can be found in the Supplementary Information of Ref. 43, from which we also took the input parameters used for CCO: these are listed in Table II. For PNO, on the other hand, the hopping integrals were reduced to 80% of their corresponding CCO values, to account for the increased  $d-p$  splitting [6]. The splittings  $\epsilon_{\pi\sigma}$  and  $\epsilon_{xy}$  values were taken from electronic structure calculations [6], as well as those of the Mott  $U$  and the Hund coupling  $J_H$  [5, 25]. For the Charge-Transfer energy  $\Delta$  there is no univocal agreement in literature, so we chose a value sufficiently larger than  $U$  also providing reasonable results. Table III compares the calculated values with those extracted from the orbital dispersion fitting 1. For the nickelate, we notice that the experimental  $J^{orb}$  agrees with the calculated orbital NN coupling: therefore, this is likely the dominant mechanism of orbital propagation, while the NNN coupling is about two orders of magnitude lower. For CCO, the scenario looks different: since the NN coupling is hindered by the coupling to magnetic excitations and the magnetic string effect, the NNN orbital superexchange actually takes over and changes the sign of the orbital dispersion. As a final remark, we mention that one of the model hypotheses in Ref. 43 is the small value of the charge transfer  $\Delta$  in the infinite-layer cuprate with respect to other cuprates, due to the absence of apical oxygens. In infinite-layer nickelates, however,  $\Delta$  is significantly larger than in any cuprate, yet we still observe the same phenomenon. This suggests that the general model may require some refinement, particularly regarding the role of the ligand in the orbital superexchange coupling.

To summarize, our comparative study of the spin, charge and orbital excitations in IL nickelates and cuprates uncovers key similarities and distinctions that shed new light on their correlated electronic states. In IL nickelates,

Parameter (eV)	PNO	CCO
$t_{pd\sigma}$	1.04	1.30
$t_{pd\pi}$	0.56	0.70
$t_{pp}$	0.56	0.70
$\Delta$	8.00	1.80
$\epsilon_{\pi\sigma}$	-1.00	-1.60
$\epsilon_{xy}$	0.70	1.00
$U$	3.20	8.00
$J_H$	0.65	1.00

TABLE II. **Microscopic parameters.** Charge transfer model parameters (in eV) employed for the calculation of  $J_{NN}^{orb}$  and  $J_{NNN}^{orb}$  (see Ref. 43 for the model details).

$J^{orb}$ (meV)	PNO	CCO
Theory $J_{NN}^{orb}$	14.5	22.0
Theory $J_{NNN}^{orb}$	$\sim -0.1$	-15.0
Experimental	$14 \pm 4$	$-11 \pm 2$

TABLE III. **Orbital superexchange values.** Calculated values of the nearest and next-nearest orbital superexchange  $J$  (in meV) for PNO and CCO, compared to those extracted from the fittings in Figure 5 (a)-(c).

in-plane hopping integrals are smaller than in cuprates, leading to approximately half the nearest neighbor exchange interaction and to a substantially lower energy of the  $d_{xy}$  excitation. However, in both families the absence of apical oxygens causes significant long-range hopping integrals, that shape the magnon in-plane dispersion and give rise to dispersing orbital excitations. The inter-plane direct exchange interaction seems little affected by the presence of a rare earth as in IL nickelates or of an alkali metal ion as in cuprates. In both cases, the out-of-plane coupling generates 3D antiferromagnetism in the IL compounds. The rare-earth in the nickelates leads to a more tridimensional electronic structure and to self-doping effects resulting in a charge continuum that merges with  $dd$  excitations in RIXS spectra. The orbital dispersion in the IL nickelate seems to primarily involve nearest neighbor orbital superexchange interaction, which in cuprates is strongly hampered by coupling to magnons. Combining these observations, we can speculate that IL nickelates are indeed mimicking the essential physics of cuprates, including the mechanisms for superconducting pairing. The lower  $T_c$  in IL nickelates is mainly due to the overall smaller energy of spin fluctuations, which can be traced back to larger charge transfer  $\Delta$  and/or smaller hopping integrals. In addition, the Mott-Hubbard nature of the correlation in IL nickelates, that cause a stronger localization of the doping charge on the metal site, might imply also a smaller electron-phonon interaction and the lack of charge density waves and fluctuations ubiquitous in hole doped cuprates. In conclusion, the fact that IL nickelates share with cuprates a wealth of properties, although with reduced interaction energies, and that the rare-earth allows in nickelates a doping mechanisms impossible in IL cuprates in the absence of apical oxygens, indicates that IL nickelates are indeed unconventional superconductors very similar to cuprates, but lacking some of the ingredients that boost  $T_c$  in cuprates.

### III. METHODS

Pristine perovskite  $\text{PrNiO}_3$  thin films were grown by RHEED-monitored Pulsed Laser Deposition on a  $\text{SrTiO}_3$  (001) substrate (STO), up to a thickness of 15-20 unit cells ( $\sim 5$  nm), and capped with an epitaxial STO layer grown in-situ up to 12 unit cells ( $\sim 3$  nm). Superconductive IL phase  $\text{PrNiO}_2$  was then obtained via a topotactic chemical reduction, consisting in the deintercalation of apical oxygen atoms by means of a high- $T$  annealing in hydrogen-rich atmosphere issued from a  $\text{CaH}_2$  powder, as done in previous studies [70–74]. The resulting samples show a complete superconducting behavior below  $T_c = 4$  K, while the SC onset (maximum curvature in the resistivity  $\rho(T)$ ) is located slightly below 11 K. The lattice parameters for the IL phase were found to be  $a = 3.94$  Å and  $c = 3.28$  Å. More details about sample growth and characterization are available in Ref. 40. The CCO films were grown by pulsed-laser deposition (KrF excimer laser,  $\lambda = 248$  nm) at a temperature around  $600^\circ\text{C}$  and an oxygen pressure of 0.1 mbar, on  $\text{NdGaO}_3$  (NGO) (1 1 0) substrate. The substrate holder was at a distance of 2.5 cm from the CCO target, which was prepared by a standard solid-state reaction [41, 42]. The lattice constants for CCO, as determined from XRD,

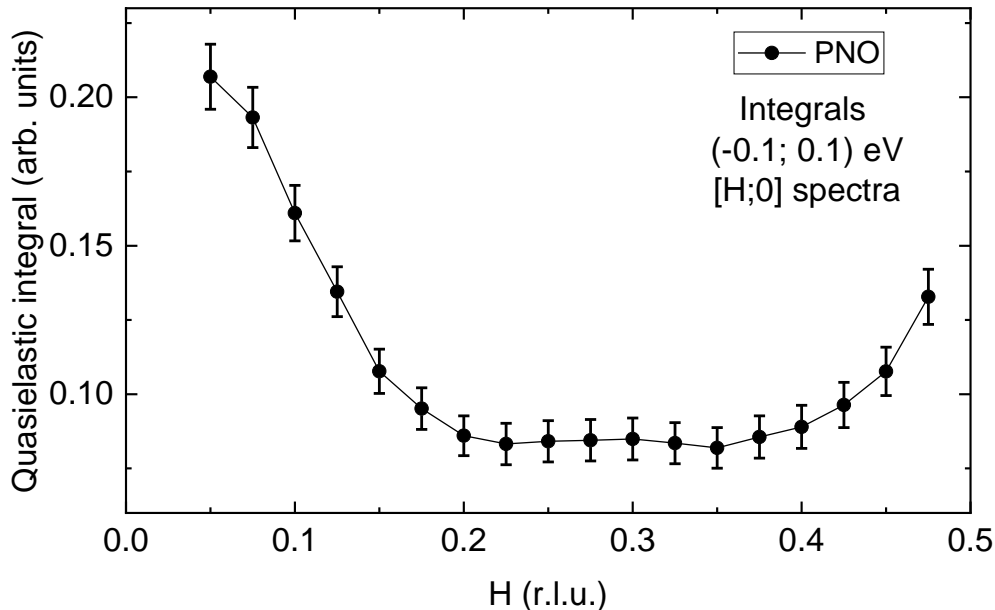


Fig. S6. **Absence of charge order.** Integrals of  $[H;0]$  spectra of PNO (figure 1(b) in the main text) on the quasielastic energy range  $[-0.1;0-1]$  eV. Error bars are given from shot noise estimation in the experimental spectra, evaluated as  $\sigma \propto \sqrt{\text{Single Photon Counting}}$ .

are  $a = b = 3.86 \text{ \AA}$  and  $c = 3.18 \text{ \AA}$ . The measured sheet resistance of CCO at room temperature (300 K) was 2 m $\Omega$ , corresponding to a resistivity of  $\sim 6000 \text{ m}\Omega\cdot\text{cm}$ . Below 250 K, the film resistance exceeded the upper limit of our measurement setup [43].

RIXS measurements were performed with the ERIXS spectrometer at the ID32 beamline of the European Synchrotron (ESRF), in Grenoble [75]. The beamline and spectrometer combined resolution was 40 meV at the Ni  $L_3$  edge (852.4 eV) of PNO and 42 meV at the Cu  $L_3$  edge (930.6 eV) of CCO. We measured momentum-resolved RIXS maps on both materials along the  $M - \Gamma - X - M$  cuts of the BZ; for PNO, the Ni- $L_3$  resonance energy is actually not enough to reach the  $X$  point, so we stopped at  $\mathbf{Q} = (0.475, 0)$  (see the inset of Figure 1(d)). We used  $\pi$  linear incident polarization and near grazing emission geometry (positive values of  $H$ ), to enhance the spin non-conserving cross-section versus the spin conserving ones [63, 76, 77]. Selected spectra were taken with polarization resolution of the scattered photons [62, 75, 78]. In this case we employed both grazing incidence ( $\theta = 24^\circ$  as measured from the sample surface) and grazing emission ( $\theta = 125^\circ$ ) geometry, both with  $\pi$  and  $\sigma$  incident polarizations. All data were collected at  $T = 20 \text{ K}$  with a fixed scattering angle  $2\theta = 149.5^\circ$ ; therefore the value of the out-of-plane momentum component  $L$  was not fixed when scanning the in plane components  $H$  and  $K$ . This is not an issue, since the in-plane exchange  $J_s$  are still dominating the out-of-plane  $J_\perp$ .

All fittings were carried out with the software Matlab. The library SpinW [58] was used for the extraction of the exchange couplings  $J_x$  from the magnetic dispersion relations. For the orbital dispersion, calculation of theoretical  $J_{NN}^{orb}$  and  $J_{NNN}^{orb}$  was based on the same charge transfer model reported in the Supplementary Information of Reference 43.

## IV. SUPPLEMENTARY MATERIAL

### A. Absence of charge order

The quasi elastic integrals of the  $[H;0]$  spectra of PNO are reported in figure S6. No detectable intensity increase is present around the wavevector  $\mathbf{Q} = [1/3;0]$ , where charge order in IL nickelates is supposed to appear [45, 52, 54].

## B. RIXS spectra fitting

Low-energy RIXS fittings reported in Figure 2(a-b) in the main text were carried out by employing two Gaussian functions for the elastic and phonon peak. As explained, the magnon was fitted with a damped harmonic oscillator function [49]: we consider that here a single-peak fit is accurate enough for our scopes, although for CCO it results in an overestimation of the single-magnon damping energy close to (0.5,0). In PNO, another broad Gaussian on the right accounts for the tail of higher-energy features, mainly the lowest-energy  $dd$  and the RE hybridization peak at 0.6 eV [11]. For CCO we also employed an antisymmetrized exponential starting at 0.3 eV to take into account multiple magnetic excitations (bimagnons), and a Gaussian for the phonon overtone (biphonon). Such higher order peaks are not independently included in the PNO fit, because these features are too close in energy and too broad. Our antisymmetrization process started from a simple Gaussian:

$$G(I, E, \sigma, x) = I e^{-\frac{x-E}{2\sigma^2}}; \quad (2)$$

where  $E, I, \sigma$  are the fitting parameters and  $x$  is the energy loss variable. A symmetric copy with respect to  $x = 0$  was then subtracted, and the resulting odd-symmetric function was then summed to its absolute value and divided by 2. As a result, we obtain a continuous curve, that is identically null for  $x \leq 0$ :

$$Y(I, E, \sigma, x) = \frac{G(I, E, \sigma, x) - G(I, -E, \sigma, x) + \left| G(I, E, \sigma, x) - G(I, -E, \sigma, x) \right|}{2} \quad (3)$$

Finally, the curve was translated rightwards to make it start from 0.2 – 0.3 eV, which is the typical energy for multiple magnetic excitations in cuprates. The precise starting point was fixed slightly differently for different spectra, according to the quality of the resulting fit.

For fittings of the  $dd$  orbital peaks, Voigt profiles antisymmetrized in a similar way were employed (Figure 2(c-d) in the main text).

- 
- [1] E. Fradkin, S. A. Kivelson, and J. M. Tranquada, Colloquium: Theory of intertwined orders in High Temperature Superconductors, *Rev. Mod. Phys.* **87**, 457 (2015).
  - [2] B. Keimer, S. A. Kivelson, M. R. Norman, S. Uchida, and J. Zaanen, From quantum matter to high-temperature superconductivity in copper oxides, *Nature* **518**, 179 (2015).
  - [3] J. Zaanen and G. Sawatzky, Systematics in band gaps and optical spectra of 3d Transition Metal compounds, *Journ. of Sol. St. Chem.* **88**, 8 (1990).
  - [4] A. S. Botana, K.-W. Lee, M. R. Norman, V. Pardo, and W. E. Pickett, Low valence Nickelates: Launching the Nickel age of Superconductivity, *Front. in Phys.* **9**, 813532 (2022).
  - [5] M. Kitatani, L. Si, O. Janson, R. Arita, Z. Zhong, and K. Held, Nickelate superconductors — a renaissance of the one-band Hubbard model, *Nat. Phys. Journ. - Quantum Mat.* **5**, 59 (2020).
  - [6] A. S. Botana and M. R. Norman, Similarities and differences between  $\text{LaNiO}_2$  and  $\text{CaCuO}_2$  and implications for Superconductivity, *Phys. Rev. X* **10**, 011024 (2020).
  - [7] Y. Nomura and R. Arita, Superconductivity in Infinite-Layer Nickelates, *Rep. of Progr. in Phys.* **85**, 052501 (2022).
  - [8] P. Jiang, L. Si, Z. Liao, and Z. Zhong, Electronic structure of Rare-Earth Infinite-Layer  $\text{RNiO}_2$  ( $R = \text{La, Nd}$ ), *Phys. Rev. B* **100**, 201106 (2019).
  - [9] B. H. Goodge, D. Li, K. Lee, M. Osada, B. Y. Wang, G. A. Sawatzky, H. Y. Hwang, and L. F. Kourkoutis, Doping evolution of the Mott–Hubbard landscape in Infinite-Layer Nickelates, *Proc. Nat. Acad. Sc.* **118**, e2007683118 (2021).
  - [10] S. Zeng, C. S. Tang, X. Yin, C. Li, M. Li, Z. Huang, J. Hu, W. Liu, G. J. Omar, H. Jani, *et al.*, Phase diagram and Superconducting dome of Infinite-Layer  $\text{Nd}_{1-x}\text{Sr}_x\text{NiO}_2$  Thin Films, *Phys. Rev. Lett.* **125**, 147003 (2020).
  - [11] M. Hepting, D. Li, C. Jia, H. Lu, E. Paris, Y. Tseng, X. Feng, M. Osada, E. Been, Y. Hikita, *et al.*, Electronic structure of the parent compound of Superconducting Infinite-Layer Nickelates, *Nat. Mat.* **19**, 381 (2020).
  - [12] H. Lu, M. Rossi, A. Nag, M. Osada, D. Li, K. Lee, B. Wang, M. Garcia-Fernandez, S. Agrestini, Z. Shen, *et al.*, Magnetic excitations in Infinite-Layer nickelates, *Science* **373**, 213 (2021).
  - [13] R. A. Ortiz, P. Puphal, M. Klett, F. Hotz, R. K. Kremer, H. Trepka, M. Hemmida, H.-A. K. von Nidda, M. Isobe, R. Khasanov, *et al.*, Magnetic correlations in Infinite-Layer Nickelates: an experimental and theoretical multimethod study, *Phys. Rev. R* **4**, 023093 (2022).
  - [14] D. Li, K. Lee, B. Y. Wang, M. Osada, S. Crossley, H. R. Lee, Y. Cui, Y. Hikita, and H. Y. Hwang, Superconductivity in an Infinite-Layer Nickelate, *Nature* **572**, 624 (2019).

- [15] S. Zeng, C. Li, L. E. Chow, Y. Cao, Z. Zhang, C. S. Tang, X. Yin, Z. S. Lim, J. Hu, P. Yang, *et al.*, Superconductivity in Infinite-Layer Nickelate  $\text{La}_{1-x}\text{Ca}_x\text{NiO}_2$  Thin Films, *Sc. Adv.* **8**, eabl9927 (2022).
- [16] S. Chow, Z. Luo, and A. Ariando, Bulk superconductivity near 40 K in hole-doped  $\text{SmNiO}_2$  at ambient pressure, *Nature* **642**, 58 (2025).
- [17] M. Osada, B. Y. Wang, B. H. Goodge, S. P. Harvey, K. Lee, D. Li, L. F. Kourkoutis, and H. Y. Hwang, Nickelate Superconductivity without Rare-Earth magnetism:  $(\text{La},\text{Sr})\text{NiO}_2$ , *Adv. Mat.* **33**, 2104083 (2021).
- [18] M. Osada, B. Y. Wang, B. H. Goodge, K. Lee, H. Yoon, K. Sakuma, D. Li, M. Miura, L. F. Kourkoutis, and H. Y. Hwang, A superconducting praseodymium nickelate with infinite layer structure, *Nano lett.* **20**, 5735 (2020).
- [19] Y. Zhou, D. Zhao, B. Zeng, C. Xia, Y. Wang, H. Chen, T. Wu, and X. Chen, Origin of local Magnetic exchange interaction in infinite-layer Nickelates, *arXiv preprint arXiv:2505.09476* (2025).
- [20] H. DahabDahab, A. Chiron, E. Tailleux, A. Largeteau, E. Durand, F. Weill, V. M. Kovrugin, S. Vasala, P. Glatzel, E. Suard, *et al.*, Unveiling the Key Role of Rare-Earth (La versus Nd) in  $\text{Ni}^+$ -Based Layered Nickelates: Impact on Structures and Physical Properties, *Chem. Mat.* (2025).
- [21] M. Rossi, H. Lu, A. Nag, D. Li, M. Osada, K. Lee, B. Y. Wang, S. Agrestini, M. Garcia-Fernandez, J. Kas, *et al.*, Orbital and spin character of doped carriers in Infinite-Layer Nickelates, *Phys. Rev. B* **104**, L220505 (2021).
- [22] G. Krieger, H. Sahib, F. Rosa, M. Rath, Y. Chen, A. Raji, P. Pinho, C. Lefevre, G. Ghiringhelli, A. Gloter, *et al.*, Signatures of canted Antiferromagnetism in Infinite-Layer Nickelates studied by X-ray Magnetic dichroism, *Phys. Rev. B* **110**, 195110 (2024).
- [23] K.-W. Lee and W. Pickett, Infinite-Layer  $\text{LaNiO}_2$ :  $\text{Ni}^{1+}$  is not  $\text{Cu}^{2+}$ , *Phys. Rev. B* **70**, 165109 (2004).
- [24] E. Been, W.-S. Lee, H. Y. Hwang, Y. Cui, J. Zaanen, T. Devereaux, B. Moritz, and C. Jia, Electronic structure trends across the Rare-Earth series in Superconducting Infinite-Layer Nickelates, *Phys. Rev. X* **11**, 011050 (2021).
- [25] P. Worm, L. Si, M. Kitatani, R. Arita, J. M. Tomczak, and K. Held, Correlations tune the electronic structure of pentalayer nickelates into the superconducting regime, *Phys. Rev. Mat.* **6**, L091801 (2022).
- [26] J. Zaanen, G. Sawatzky, and J. Allen, Band gaps and Electronic structure of Transition-Metal compounds, *Phys. Rev. Lett.* **55**, 418 (1985).
- [27] Z. Chen, M. Osada, D. Li, E. M. Been, S.-D. Chen, M. Hashimoto, D. Lu, S.-K. Mo, K. Lee, B. Y. Wang, *et al.*, Electronic structure of Superconducting Nickelates probed by Resonant Photoemission Spectroscopy, *Matter* **5**, 1806 (2022).
- [28] V. Bisogni, S. Catalano, R. J. Green, M. Gibert, R. Scherwitzl, Y. Huang, V. N. Strocov, P. Zubko, S. Balandeh, J.-M. Triscone, *et al.*, Ground-state oxygen holes and the Metal-Insulator Transition in the negative Charge-Transfer Rare-Earth Nickelates, *Nat. Comm.* **7**, 13017 (2016).
- [29] J. Kapeghian and A. S. Botana, Electronic structure and Magnetism in Infinite-Layer Nickelates  $\text{RNiO}_2$  ( $\text{R} = \text{La-Lu}$ ), *Phys. Rev. B* **102**, 205130 (2020).
- [30] Y.-f. Yang and G.-M. Zhang, Self-doping and the Mott-Kondo scenario for Infinite-Layer Nickelate Superconductors, *Front. in Phys.* **9**, 801236 (2022).
- [31] G.-M. Zhang, Y.-f. Yang, and F.-C. Zhang, Self-doped Mott insulator for parent compounds of Nickelate Superconductors, *Phys. Rev. B* **101**, 020501 (2020).
- [32] F. Lechermann, Late Transition Metal Oxides with Infinite-Layer structure: Nickelates versus Cuprates, *Phys. Rev. B* **101**, 081110 (2020).
- [33] Y. Nomura, M. Hirayama, T. Tadano, Y. Yoshimoto, K. Nakamura, and R. Arita, Formation of a two-dimensional single-component correlated electron system and band engineering in the nickelate superconductor  $\text{NdNiO}_2$ , *Phys. Rev. B* **100**, 205138 (2019).
- [34] X. Ding, Y. Fan, X. Wang, C. Li, Z. An, J. Ye, S. Tang, M. Lei, X. Sun, N. Guo, *et al.*, Cuprate-like electronic structures in infinite-layer nickelates with substantial hole dopings, *Nat. Sc. Rev.* **11**, nwae194 (2024).
- [35] C. Li, Y. Chen, X. Ding, Y. Zhuang, N. Guo, Z. Chen, Y. Fan, J. Ye, Z. An, S. Sangphet, *et al.*, Observation of electridelike  $s$  states coexisting with Correlated  $d$  electrons in  $\text{NdNiO}_2$ , *Phys. Rev. Lett.* **135**, 116501 (2025).
- [36] P. Worm, Q. Wang, M. Kitatani, I. Bialo, Q. Gao, X. Ren, J. Choi, D. Csontosová, K.-J. Zhou, X. Zhou, *et al.*, Spin fluctuations sufficient to mediate Superconductivity in Nickelates, *Phys. Rev. B* **109**, 235126 (2024).
- [37] D. J. Scalapino, A common thread: The pairing interaction for unconventional Superconductors, *Rev. Mod. Phys.* **84**, 1383 (2012).
- [38] D. R. Saykin, M. Gonzalez, J. Fowlie, S. A. Kivelson, H. Y. Hwang, and A. Kapitulnik, Spin-glass state in Nickelate Superconductors, *Nat. Phys. Journ. - Quantum Mat.* **10**, 94 (2025).
- [39] J. Fowlie, M. Hadjimichael, M. M. Martins, D. Li, M. Osada, B. Y. Wang, K. Lee, Y. Lee, Z. Salman, T. Prokscha, *et al.*, Intrinsic magnetism in Superconducting Infinite-Layer Nickelates, *Nat. Phys.* **18**, 1043 (2022).
- [40] H. Sahib, A. Raji, F. Rosa, G. Merzoni, G. Ghiringhelli, M. Salluzzo, A. Gloter, N. Viart, and D. Preziosi, Superconductivity in  $\text{PrNiO}_2$  Infinite-Layer Nickelates, *Adv. Mat.* **37**, 2416187 (2025).
- [41] E. Stellino, P. Postorino, S. Sanna, A. Tebano, and D. Di Castro, On the role of strain-and doping-induced disorder in epitaxial  $\text{CaCuO}_2$  films: Lattice and spin dynamics in light scattering response, *Journ. of Appl. Phys.* **137** (2025).
- [42] D. Di Castro, C. Cantoni, F. Ridolfi, C. Aruta, A. Tebano, N. Yang, and G. Balestrino, High- $T_c$  superconductivity at the interface between the  $\text{CaCuO}_2$  and  $\text{SrTiO}_3$  insulating oxides, *Phys. Rev. Lett.* **115**, 147001 (2015).
- [43] L. Martinelli, K. Wohlfeld, J. Pellicciari, R. Arpaia, N. B. Brookes, D. Di Castro, M. G. Fernandez, M. Kang, Y. Krockenberger, K. Kummer, *et al.*, Collective nature of orbital excitations in layered cuprates in the absence of apical oxygens, *Phys. Rev. Lett.* **132**, 066004 (2024).
- [44] M. Moretti Sala, V. Bisogni, C. Aruta, G. Balestrino, H. Berger, N. Brookes, G. De Luca, D. Di Castro, M. Grioni, M. Guarise, *et al.*, Energy and symmetry of  $dd$  excitations in undoped layered cuprates measured by  $\text{Cu } L_3$  Resonant

- Inelastic X-ray Scattering, *New Journ. of Phys.* **13**, 043026 (2011).
- [45] G. Krieger, L. Martinelli, S. Zeng, L. E. Chow, K. Kummer, R. Arpaia, M. M. Sala, N. B. Brookes, A. Ariando, N. Viart, M. Salluzzo, G. Ghiringhelli, and D. Preziosi, Charge and Spin Order Dichotomy in  $\text{NdNiO}_2$  Driven by the Capping Layer, *Phys. Rev. Lett.* **129**, 27002 (2022).
- [46] F. Rosa, L. Martinelli, G. Krieger, L. Braicovich, N. B. Brookes, G. Merzoni, M. Moretti Sala, F. Yakhou-Harris, R. Arpaia, D. Preziosi, *et al.*, Spin Excitations in  $\text{Nd}_{1-x}\text{Sr}_x\text{NiO}_2$  and  $\text{YBa}_2\text{Cu}_3\text{O}_{7-\delta}$ : The influence of Hubbard  $U$ , *Phys. Rev. B* **110**, 224431 (2024).
- [47] M. Rossi, H. Lu, K. Lee, B. Goodge, J. Choi, M. Osada, Y. Lee, D. Li, B. Wang, D. Jost, *et al.*, Universal orbital and Magnetic structures in Infinite-Layer Nickelates, *Phys. Rev. B* **109**, 024512 (2024).
- [48] Y. Peng, G. Dellea, M. Minola, M. Conni, A. Amorese, D. Di Castro, G. De Luca, K. Kummer, M. Salluzzo, X. Sun, *et al.*, Influence of apical oxygen on the extent of in-plane exchange interaction in Cuprate Superconductors, *Nat. Phys.* **13**, 1201 (2017).
- [49] Y. Peng, E. Huang, R. Fumagalli, M. Minola, Y. Wang, X. Sun, Y. Ding, K. Kummer, X. Zhou, N. Brookes, *et al.*, Dispersion, damping, and intensity of Spin Excitations in the Monolayer  $(\text{Bi,Pb})_2(\text{Sr,Lu})_2\text{CuO}_{6+\delta}$  Cuprate superconductor family, *Phys. Rev. B* **98**, 144507 (2018).
- [50] L. Martinelli, D. Betto, K. Kummer, R. Arpaia, L. Braicovich, D. Di Castro, N. B. Brookes, M. Moretti Sala, and G. Ghiringhelli, Fractional Spin Excitations in the Infinite-Layer Cuprate  $\text{CaCuO}_2$ , *Phys. Rev. X* **12**, 021041 (2022).
- [51] L. Braicovich, L. Ament, V. Bisogni, F. Forte, C. Aruta, G. Balestrino, N. Brookes, G. De Luca, P. Medaglia, F. M. Granozio, *et al.*, Dispersion of Magnetic excitations in the Cuprate  $\text{La}_2\text{CuO}_4$  and  $\text{CaCuO}_2$  compounds measured using resonant X-ray Scattering, *Phys. Rev. Lett.* **102**, 167401 (2009).
- [52] M. Rossi, M. Osada, J. Choi, S. Agrestini, D. Jost, Y. Lee, H. Lu, B. Y. Wang, K. Lee, A. Nag, *et al.*, A broken translational symmetry state in an Infinite-Layer Nickelate, *Nat. Phys.* **18**, 869 (2022).
- [53] C. C. Tam, J. Choi, X. Ding, S. Agrestini, A. Nag, M. Wu, B. Huang, H. Luo, P. Gao, M. García-Fernández, *et al.*, Charge Density Waves in Infinite-Layer  $\text{NdNiO}_2$  Nickelates, *Nat. Mat.* **21**, 1116 (2022).
- [54] C. T. Parzyk, N. K. Gupta, Y. Wu, V. Anil, L. Bhatt, M. Bouliane, R. Gong, B. Gregory, A. Luo, R. Sutarto, *et al.*, Absence of  $3a_0$  Charge Density Wave order in the Infinite-Layer Nickelate  $\text{NdNiO}_2$ , *Nat. Mat.* **23**, 486 (2024).
- [55] B. Dalla Piazza, M. Mourigal, N. B. Christensen, G. Nilsen, P. Tregenna-Piggott, T. Perring, M. Enderle, D. F. McMorrow, D. Ivanov, and H. M. Rønnow, Fractional excitations in the square-lattice quantum antiferromagnet, *Nat. Phys.* **11**, 62 (2015).
- [56] D. Betto, R. Fumagalli, L. Martinelli, M. Rossi, R. Piombo, K. Yoshimi, D. Di Castro, E. Di Gennaro, A. Sambri, D. Bonn, *et al.*, Multiple-Magnon excitations shape the spin spectrum of Cuprate parent compounds, *Phys. Rev. B* **103**, L140409 (2021).
- [57] R. Coldea, S. Hayden, G. Aeppli, T. Perring, C. Frost, T. Mason, S.-W. Cheong, and Z. Fisk, Spin Waves and Electronic interactions in  $\text{La}_2\text{CuO}_4$ , *Phys. Rev. Lett.* **86**, 5377 (2001).
- [58] *SpinW* software.
- [59] Q. Gao, S. Fan, Q. Wang, J. Li, X. Ren, I. Bialo, A. Drewanowski, P. Rothenbühler, J. Choi, R. Sutarto, *et al.*, Magnetic excitations in strained Infinite-Layer Nickelate  $\text{PrNiO}_2$  films, *Nat. Comm.* **15**, 5576 (2024).
- [60] Y. Yan, Y. Chan, X. Hong, S. Chow, Z. Luo, Y. Li, T. Wang, Y. Wu, I. Bialo, N. Fitriyah, *et al.*, Persistent paramagnons in high-temperature infinite-layer nickelate superconductors, *arXiv preprint arXiv:2507.18373* (2025).
- [61] I. Bialo, L. Martinelli, G. De Luca, P. Worm, A. Drewanowski, S. Jöhr, J. Choi, M. Garcia-Fernandez, S. Agrestini, K.-J. Zhou, *et al.*, Strain-tuned incompatible Magnetic exchange-interaction in  $\text{La}_2\text{NiO}_4$ , *Comm. Phys.* **7**, 230 (2024).
- [62] R. Fumagalli, L. Braicovich, M. Minola, Y. Peng, K. Kummer, D. Betto, M. Rossi, E. Lefrançois, C. Morawe, M. Salluzzo, *et al.*, Polarization-resolved Cu  $L_3$ -edge Resonant Inelastic X-ray Scattering of orbital and Spin Excitations in  $\text{NdBa}_2\text{Cu}_3\text{O}_{7-\delta}$ , *Phys. Rev. B* **99**, 134517 (2019).
- [63] L. J. Ament, G. Ghiringhelli, M. M. Sala, L. Braicovich, and J. van den Brink, Theoretical demonstration of how the dispersion of Magnetic excitations in Cuprate compounds can be determined using Resonant Inelastic X-ray Scattering, *Phys. Rev. Lett.* **103**, 117003 (2009).
- [64] J.-i. Igarashi and T. Nagao, Magnetic excitations in  $L$ -edge Resonant Inelastic X-ray Scattering from Cuprate compounds, *Phys. Rev. B - Cond. Matt. and Mater. Phys.* **85**, 064421 (2012).
- [65] J. Schlappa, K. Wohlfeld, K. Zhou, M. Mourigal, M. Haverkort, V. Strocov, L. Hozoi, C. Monney, S. Nishimoto, S. Singh, *et al.*, Spin-Orbital separation in the quasi-one-dimensional Mott insulator  $\text{Sr}_2\text{CuO}_3$ , *Nature* **485**, 82 (2012).
- [66] R. Fumagalli, J. Heverhagen, D. Betto, R. Arpaia, M. Rossi, D. Di Castro, N. B. Brookes, M. Moretti Sala, M. Daghofer, L. Braicovich, *et al.*, Mobile orbitons in  $\text{Ca}_2\text{CuO}_3$ : Crucial role of Hund's exchange, *Phys. Rev. B* **101**, 205117 (2020).
- [67] D. I. Khomskii, *Transition Metal Compounds* (Cambridge University Press, 2014).
- [68] K. Wohlfeld, M. Daghofer, G. Khaliullin, and J. van den Brink, Dispersion of orbital excitations in 2D quantum antiferromagnets, *Journ. of Phys.: Conference Series* **391**, 012168 (2012).
- [69] K. Wohlfeld, M. Daghofer, S. Nishimoto, G. Khaliullin, and J. van den Brink, Intrinsic coupling of orbital excitations to spin fluctuations in Mott insulators, *Phys. Rev. Lett.* **107**, 147201 (2011).
- [70] K. Lee, B. H. Goodge, D. Li, M. Osada, B. Y. Wang, Y. Cui, L. F. Kourkoutis, and H. Y. Hwang, Aspects of the synthesis of Thin Film Superconducting Infinite-Layer Nickelates, *APL Materials* **8** (2020).
- [71] G. Krieger, A. Raji, L. Schlur, G. Versini, C. Bouillet, M. Lenertz, J. Robert, A. Gloter, N. Viart, and D. Preziosi, Synthesis of Infinite-Layer Nickelates and influence of the capping-layer on magnetotransport, *Journ. of Phys. D: Appl. Physics* **56**, 024003 (2023).
- [72] P. Puphal, B. Wehinger, J. Nuss, K. Küster, U. Starke, G. Garbarino, B. Keimer, M. Isobe, and M. Hepting, Synthesis

and physical properties of  $\text{LaNiO}_2$  crystals, *Phys. Rev. Mat.* **7**, 014804 (2023).

- [73] M. Hayward, M. Green, M. Rosseinsky, and J. Sloan, Sodium hydride as a powerful reducing agent for topotactic oxide deintercalation: synthesis and characterization of the Nickel(I) oxide  $\text{LaNiO}_2$ , *Journ. of the Amer. Chem. Soc.* **121**, 8843 (1999).
- [74] M. Hayward and M. Rosseinsky, Synthesis of the infinite layer Ni(I) phase  $\text{NdNiO}_{2+x}$  by low temperature reduction of  $\text{NdNiO}_3$  with sodium hydride, *Solid State Sciences* **5**, 839 (2003).
- [75] N. B. Brookes, F. Yakhou-Harris, K. Kummer, A. Fondacaro, J. Cezar, D. Betto, E. Velez-Fort, A. Amorese, G. Ghiringhelli, L. Braicovich, *et al.*, The beamline ID32 at the ESRF for soft X-ray high energy resolution resonant inelastic X-ray scattering and polarisation dependent X-ray absorption spectroscopy, *Nucl. Instr. and Meth. in Phys. Res. - Section A* **903**, 175 (2018).
- [76] L. Braicovich, M. M. Sala, L. Ament, V. Bisogni, M. Minola, G. Balestrino, D. Di Castro, G. De Luca, M. Salluzzo, G. Ghiringhelli, *et al.*, Momentum and Polarization Dependence of Single-Magnon Spectral Weight for Cu  $L_3$ -edge Resonant Inelastic X-ray Scattering from Layered Cuprates, *Phys. Rev. B* **81**, 174533 (2010).
- [77] M. Haverkort, Theory of Resonant Inelastic X-ray Scattering by collective Magnetic excitations, *Phys. Rev. Lett.* **105**, 167404 (2010).
- [78] L. Braicovich, M. Minola, G. Dellea, M. Le Tacon, M. Moretti Sala, C. Morawe, J.-C. Peffen, R. Suprunganet, F. Yakhou, G. Ghiringhelli, *et al.*, The simultaneous measurement of Energy and Linear Polarization of the Scattered Radiation in Resonant Inelastic soft X-ray Scattering, *Rev. of Scient. Instr.* **85** (2014).

## V. FUNDING INFORMATION

F.R., G.M., L.M., M.Z., M.S. and G.G. acknowledge support by the projects PRIN2017 Quantum-2D-ID 2017Z8TS5Band PRIN 2020 QT-FLUO ID 20207ZXT4Z of the Ministry for University and Research (MIUR) of Italy. D.P. acknowledges the ANR-FRANCE (French National Research Agency) for its financial support of the T-ERC project ORBIFUN ANR-23-ERCS-0003-01. This work was partially performed within the MUSA-Multilayered Urban Sustainability Action project, funded by the European Union-NextGenerationEU, under the National Recovery and Resilience Plan (NRRP) Mission 4 Component 2 Investment Line 1.5: Strengthening of research structures and creation of R&D, “innovation ecosystems” set up of “territorial leaders” in R&D. The work by G.M. was jointly supported by Politecnico di Milano and European X-ray Free Electron Laser Facility GmbH.

## VI. ACKNOWLEDGMENTS

We thank Marco Moretti Sala for valuable discussion. This research used ESRF beamline ID32 under the Proposals No. HC5438, using the ERIXS spectrometer designed jointly by the ESRF and Politecnico di Milano.

## VII. AUTHOR CONTRIBUTIONS

F.R., G.M., L.M., N.B., M.S. and G.G. conceived and performed the RIXS measurements, with suggestions from R.A. and D.P. H.S. and D.P. grew and characterized the PNO thin films; D.D.C. grew and characterized the CCO films. F.R. analyzed the RIXS experimental data and performed the fittings. F.R., M.S. and G.G. discussed and interpreted the results. M.Z. performed single-ion calculations. F.R. and G.G. wrote the manuscript with major suggestions from R.A. and contributions from all authors.

## VIII. COMPETING INTERESTS

The authors declare no competing interests.